ELSEVIER

PII: S0032-3861(97)10359-7

Polymer Vol. 39 No. 16, pp. 3597–3609, 1998

0032-3861/98/$19.00+0.00

Creep behaviour of high density polyethylene films having well-defined morphologies of stacked lamellae with and without an observable row-nucleated fibril structure

Hongyi Zhou and Garth L. Wilkes*
Chemical Engineering Department, Polymer Materials and Interfaces Laboratory, Virginia Polytechnic Institute and State University, Blacksburg, VA 24061, USA
(Received 16 June 1997; revised 7 November 1997; accepted 24 November 1997)

Creep behaviour of melt-extruded high density polyethylene films, having a stacked lamellar morphology (either with or without the visible (by transmission electron microscopy, TEM) presence of row-nucleated fibril structures) and compression moulded slow-cooled isotropic films of the same resins, was investigated. The creep experiments were carried out at different temperatures and stresses, and the orientation dependence of the creep behaviour for the melt-extruded films was studied by performing the creep experiments at three angles (0°, 45° and 90°), with respect to the original machine direction. An Eyring-rate model was used to analyse the creep data, and the three parameters associated with the Eyring-rate model, i.e. activation volume, activation energy and the availability of creep sites, were obtained by fitting the plateau creep rate according to the Eyring-rate equation. It was concluded that the creep behaviour of all the films was basically controlled by the deformation of the amorphous phase and, more specifically, by the density and tautness of tie-chains. The orientation dependence on the melt-extruded films was explained by the different constraint effects of crystalline lamellae to the tie-chains at each orientation.

(Keywords: polyethylene; creep; Eyring-rate model)

INTRODUCTION

Creep is the time-dependent strain (elongation) for a material under constant stress. For polymers, creep deformation is an important and powerful experimental method to study many physical properties including viscoelastic behaviour and physical aging. On the other hand, creep is also a common phenomenon for engineering applications where products are under specified loads, and the service life of the components is a major concern. Therefore it is also critical to understand the origin of creep deformation and to be able to predict the long time creep behaviour for a given polymeric material under specific conditions.

Various empirical relations have been proposed to describe the creep behaviour of polymers[1–24]. The Andrade law, originally used for describing high temperature creep behaviour of metals in the early 1950s, has also been applied to polymers in general[1–5]. The major drawback for such power law relationships is that they do not have a fundamental basis. Another general relationship that has also been commonly used for polymers is based on the rationalization that, due to their viscoelastic nature, the response of polymers to an external constant stress contains: (1) an instantaneous elastic response; (2) a delayed (time-dependent) viscoelastic response; and (3) a permanent flow response[6–9]. This idea has led to the following phenomenological based equation

$$\epsilon(t) = \epsilon_o + \epsilon_q\left[1 - \exp\left(-\frac{t}{\tau}\right)\right] + \dot{\epsilon}_p t \qquad (1)$$

where $\epsilon(t)$ is the time-dependent creep strain at the elapsed loading time t, ϵ_o is the instantaneous strain due to the elastic response of the polymer, ϵ_q is a strain constant which is used, in conjunction with an exponential decay function having a characteristic relaxation time τ, to describe the transient viscoelastic response, and $\dot{\epsilon}_p$ is the plateau creep rate due to permanent flow. Based on equation (1), at very long loading times, the creep deformation is dominated by the plateau creep rate, which has been found to be the case in creep tests for many polymers[10]. This relation can also be coupled to the common four-element fluid mechanical analogue often used in describing the rheological and viscoelastic behaviour of polymers[5]. However, no information regarding the molecular mechanisms of creep can be extracted by this approach.

It is certain that morphology plays an important role in affecting the creep behaviour for a given polymer. For amorphous polymers, the Kohlrausch–Williams–Watts (KWW) relation, which states that creep compliance increases according to a stretched exponential function of time, has also been widely used[11], especially in the area of physical aging of glassy amorphous polymers[12]. However, the KWW relation has been found only valid for creep over limited periods of time[13]. It is also found that extrapolating creep data to longer times by using this relationship can cause large errors, even at temperatures below the glass transition temperature (T_g)[14]. In addition, the use of the KWW formula to semicrystalline polymers above their T_g has not been found to be particularly beneficial.

Most amorphous polymers are found to be thermorheologically simple at temperatures above T_g; therefore,

* To whom correspondence should be addressed

the time–temperature superposition principle has also been used in the creep study of amorphous polymers[14–16]. According to this principle, the long time creep data can be 'obtained' by performing experiments at higher temperatures in shorter time scales for the same material. For semicrystalline polymers, however, due to the complex coupling between the crystalline phase and the amorphous phase (i.e. thermorheological complexity), the time–temperature superposition principle is generally not applicable[17,18].

To address the complex dependence of creep behaviour on stress, time and temperature, other relationships have been proposed. One approach suggested that the creep strain has a power law dependence on both the loading time and applied stress, but an exponential dependence on the temperature[19]. However, there is no theoretical basis based on which these dependencies can be justified, and nor does this explain the plateau creep rate observed in many creep experiments. Another approach to describe creep behaviour has made use of the Eyring-rate model[20]. In this case, creep is considered to occur by flow-units, which may be polymer chains, segments of chains or groups of segments of chains, slipping over one another from one (metastable) position to another when stress is applied. The kinetics of this event can be expressed by the Eyring-rate model. In other words, creep is due to a molecular motion that takes place within a specific volume passing over an energy barrier. The plateau creep rate is considered to be a function of stress, time and temperature, as shown by the Eyring-rate equation

$$\dot{\epsilon}_p = \dot{\epsilon}_o \exp\left(-\frac{U}{kT}\right)\sinh\left(\frac{V\sigma}{kT}\right) \tag{2}$$

where V is the activation volume, U is the activation energy, σ is the applied stress, $\dot{\epsilon}_p$ is the plateau creep rate, the pre-exponential factor, $\dot{\epsilon}_o$, commonly known as the 'availability of event sites', is related to the fundamental jumping frequency for the flow units to bypass each other. Clearly, the merit of this approach is that the creep behaviour can often be coupled with some molecular features of the polymer of interest, such as chain chemistry, molecular weight and its distribution and morphology, which affect the mobility of chains and/or chain segments.

In the development of well-oriented high modulus polyethylene fibres, particularly ultra-high molecular weight polyethylene (UHMWPE) fibres, the creep behaviour has been found to be a major shortcoming that limits the applications of these fibres[21–25]. Thus, the creep behaviour of these fibres has been investigated extensively, especially by using the Eyring-rate approach. A creep model consisting of two thermally activated Eyring-rate processes has been proposed by Ward and coworkers[21–25]. One process has been attributed to the contribution from the crystalline phase, and it is dominant at a high stress level. The other process has been attributed to the contribution from the amorphous network, and it dominates at a low stress level. Here, the critical stress which divides the high and low stress level is about 0.2 GPa for samples used by Ward and coworkers in their investigations[22,23]. Furthermore, the higher stress process has also been regarded as the same mechanism as that of the mechanical α relaxation in linear polyethylene, i.e. a chain-to-chain slip process in the crystalline phase. The lower stress process, on the other hand, was speculated to be due to the deformation of the amorphous network in the material; however, the precise nature of this low stress process has not been addressed.

Given the long history of creep studies of polymers, there is still an apparent absence of a full understanding of the molecular creep mechanisms, especially for semicrystalline polymers. There have been some creep studies with a specific focus on the melt or solution spun high or UHMWPE fibres[9,21–25]. There have also been a limited amount of creep studies on other kinds of polymeric fibres based on aromatic chemistry (e.g. PEEK)[26,27]. In these investigations, the materials tend to possess a highly oriented extended-chain type fibril morphology. Therefore, the creep behaviour noted for these fibres is expected to be somewhat different from those for general semicrystalline polymers having an initially isotropic morphology.

In this study, the creep behaviour of melt-extruded high density polyethylene (HDPE) films having a well-defined stacked lamellar morphology, either with or without a distinct visible presence of row-nucleated fibril structure, were investigated. The creep experiments were carried out at different angles with respect to the machine direction of the films at different temperatures as well as under different applied stresses. The creep behaviour of unoriented samples of the same HDPE resins was also investigated. It is our hope that by doing a thorough investigation on materials having well-defined morphologies, the corresponding creep mechanisms can be better understood. In addition, by comparing the creep data for the same materials with a variety of morphologies due to different processing (crystallization) conditions (i.e. melt-extrusion *versus* compression moulding), a more complete understanding of the creep behaviour for semicrystalline polymers can be obtained.

EXPERIMENTAL

Materials

Two HDPE resins were used in this study. Both polymers have the same number average molecular weight of 14 500 g mol^{-1}, but they differ in weight average molecular weight, with that of Resin 1 being 150 000 g mol^{-1} and that of Resin 2 being 219 000 g mol^{-1}. More detailed information regarding the two resins as well as the melt rheological characterization of these resins has been described elsewhere[28]. The 25 micron thick melt-extruded and highly oriented HDPE films of both resins were provided by the Hoechst Celanese Corporation. The extruded film of Resin 1 (designated as Pre-1 film) has a well-defined stacked lamellar morphology, and the crystalline phase is uniaxially oriented with the polymer chains preferentially aligned along the machine direction (MD). This was quantified by determination of the Hermans' orientation function, f_c, for the crystalline phase using wide angle X-ray scattering (WAXS), where f_c is defined as

$$f_c = \frac{1}{2}(\langle\cos^2\theta\rangle - 1) \tag{3}$$

In equation (3), the quantity $\langle\cos^2\theta\rangle$ represents the average value of $\cos^2\theta$, with θ being the angle between the c-axis in the crystal (chain axis direction) and the MD. The amorphous phase, however, was essentially in a random state, as noted previously by combining the analysis of both WAXS and birefringence measurements[28]. The extruded film of Resin 2 (designated as Pre-2 film) has the presence of a visibly distinct row-nucleated fibril structure in addition to

the well stacked crystalline lamellae, as revealed by transmission electronic microscopy (TEM). The f_c values calculated form the WAXS patterns for the Pre-1 and Pre-2 films were 0.67 and 0.71, respectively. A detailed investigation of the orientation state of both the crystalline phase and the amorphous phase of the melt-extruded films of Resin 1 and Resin 2 has been published elsewhere[29]. In addition, unoriented (isotropic) compression moulded slow-cooled films (100 microns thick) of both resins were also investigated in this study, and these film are designated as HP-1 and HP-2 films accordingly.

Transmission electron microscopy

For the TEM study, samples of the melt-extruded films of Resin 1 and Resin 2 were treated by chlorosulfonic acid at 60°C for 6 h; then, they were washed with sulfuric acid and followed by water and dried overnight. The stained samples were embedded in an epoxy resin and cured at 65°C overnight. The embedded samples were microtomed at room temperature by cutting along the MD. The microtomed thin sections of *ca* 80 nm thick were used for the TEM observations after being treated by uranyl acetate. All the TEM work was performed by using a Philips EM420 instrument operated at 100 kV.

Wide angle X-ray scattering

All the WAXS experiments were performed by utilizing a Philips tabletop X-ray Generator (Model PW1720) equipped with a standard vacuum-sealed Warhus photographic pinhole camera. The instrument with a Cu–K_α radiation (= 1.54 Å) was operated at 40 kV and 20 mA. Stacks of 32 layers of films were used for each specimen for the WAXS experiments, and the exposure time used was roughly 2 h.

Tensile tests

The stress–strain curves for all the samples of melt-extruded films were obtained by using an Instron (4400 model) at ambient conditions. Dogbone shape samples of 23mm × 8mm were stretched at a cross-head speed of 15 mm min^{-1}. For the Pre-1 and Pre-2 films, the samples were cut at three different angles, 0°, 45° and 90°, with respect to the original MD, and they were denoted as 0° stretch, 45° stretch and 90° stretch, respectively.

Creep experiments

Dead-load type creep experiments was carried out by using a thermal mechanical analyser (TMA, Seiko TMA100) instrument operating in a tensile mode. For the melt-extruded films, samples for the creep experiments were rectangular stripes cut with a die of 3.2 mm wide and 25 mm long at the same three angles (0°, 45° and 90°) with respect to the original MD of the extruded films, and the creep experiments at these orientations are denoted as 0° creep, 45° creep and 90° creep, respectively. On the other hand, sample width for the compression moulded films is about 2.0 mm to keep the stress level in the creep experiments close to those used for the melt-extruded films. A different sample was used for each individual creep experiment to prevent the influence of permanent flow due to a previous loading for the sample. A sample strip was fixed within sample chucks, and then inserted into a quartz probe through which a tensile load was applied to each sample. A small initial pre-tensile load of 3 g was applied to make sure that the sample was taut. After the temperature reached the selected temperature and stabilized, which could be controlled to ± 0.3°C, a designated creep load was applied to the sample for more than 4 h (250 min). The selected temperatures were 30, 40, 50, and 60°C which cover a portion of application temperature region for HDPE products. Five different but relative small load levels of 10, 20, 40, 60 and 80 g were used in the experiments to ensure that the initial strains of the samples were below their corresponding yield strains. The elongation of the samples during the creep (TMA) experiments were monitored by a LVDT attached to the quartz probe. In addition, differential TMA signal (DTMA) was also collected. Approximately 30% of the total creep experiments were duplicated, and the data showed good reproducibility for the overall creep curves in the selected temperature and load region.

RESULTS

The TEM micrographs and WAXS patterns for the Pre-1 and Pre-2 films are presented in *Figures 1 and 2*, respectively. Since the films are essentially uniaxially oriented, the TEM micrographs taken from thin sections with their normal perpendicular to the transverse direction (*Figure 1*) can be consistently compared with WAXS

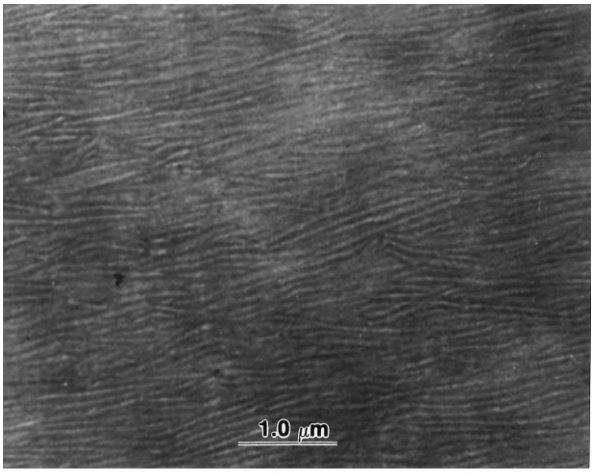

(a)

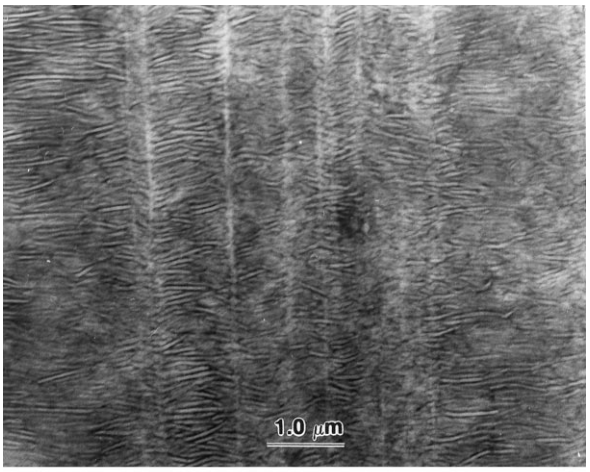

(b)

Figure 1 TEM micrographs showing the stacked lamellae for the Pre-1 film (a) and the rows structures in the matrix of stacked lamellae for the Pre-2 film (b). The MD is along the vertical direction

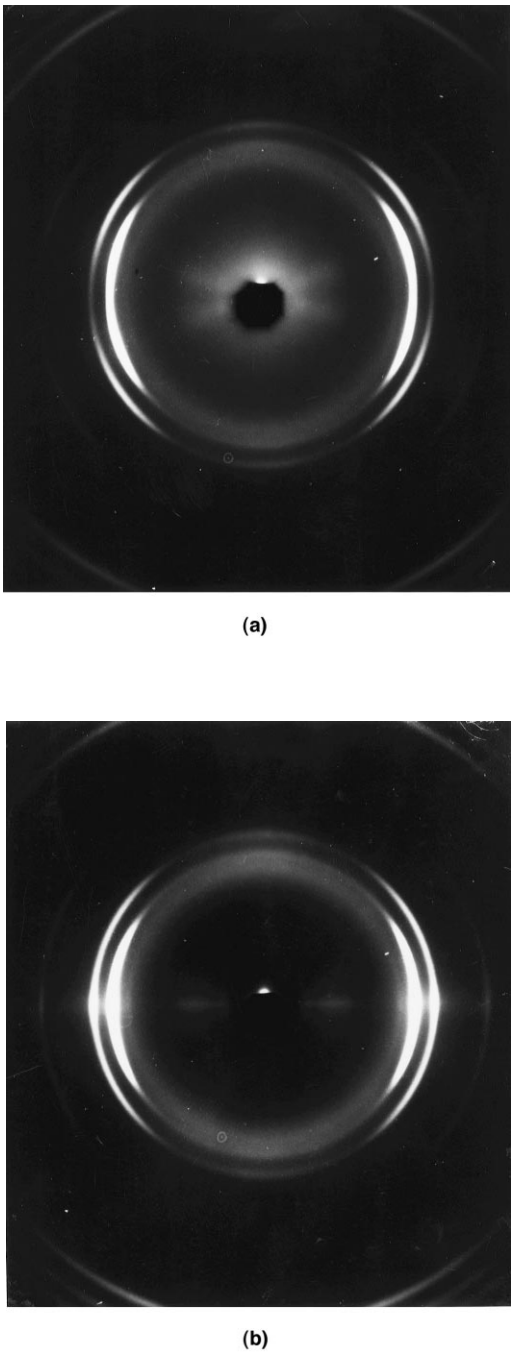

Figure 2 WAXS patterns showing the highly oriented state of the crystalline phase for the Pre-1 (a) and the Pre-2 films (b). The MD is along the vertical direction

patterns with the X-ray beam directed along the normal direction (*Figure 2*). The well-oriented and well-defined stacked lamellae for the Pre-1 film and the distinguishable amount of row-nucleated fibril structure in the matrix of stacked lamellae for the Pre-2 film are clearly revealed. A more detailed investigation on these films published elsewhere confirmed the uniaxial orientation state of the crystalline phase[29].

For the Pre-2 film, the existence of two high intensity scattering spots that superimposed on the (110) and (200) reflections in the equatorial region corresponds to the row-nucleated fibril structure in the material. However, no such extra strongly azimuthally dependent reflections were found for the Pre-1 film, which is in agreement with the TEM observations where no visible signs of fibril nuclei were noted. Slight lamellar twisting, indicated by the presence of some very weak a-axis orientation from the (200) reflection on the meridinal region of the WAXS patterns (*Figure 2*), was, however, not observed by TEM. It needs to be pointed out that the calculation of the crystalline orientation function for Resin 2 mentioned earlier did not take into account the high intensity reflection spots from this second population of very highly oriented fibril crystals. Both the TEM and WAXS experiments have been repeated by using different samples, and the above-mentioned structural features were all well reproducable.

Stress–strain behaviour

The stress–strain curves for the Pre-1 and Pre-2 films are shown in *Figure 3a* and *b*. As expected, these curves showed a distinct orientation dependence of the stress–strain behaviour of these films in terms of modulus, yielding behaviour, cold drawing, strain hardening, and fracture. These differences in mechanical properties have been correlated to unique structural changes at respective deformation directions in a detailed investigation on the deformation process of the Pre-1 and Pre-2 films has been carried out and has been published elsewhere[30]. Here, only those features that are related to the creep study are restated.

For the 0° stretch, the films from the both resins had a large degree of strain hardening that begins at about 10% strain. However, no necking was found in the entire strain range, although strain whitening did occur even before the onset of strain hardening. This change in optical clarity is caused by the splaying of the stacked lamellae. For the 90° stretch, yielding (the presence of a sharp local yield peak) took place at a very small strain (4%) and is associated with the formation of a sharp neck with boundaries perpendicular to the stretching direction. Following yielding, the samples displayed extensive cold drawing by the expansion of the neck along the samples' length. Also noticed is the uneven features of the stress–strain curves. The stress–strain curves for the 45° stretch look more typical for unoriented semicrystalline polymers with a spherulitic morphology—with yielding (at 16% by the well-defined local maximum in the stress–strain curve), strain softening, cold drawing, strain hardening, and failure. In this case, yielding took place by the formation of a neck with boundaries at 45° with respect to the stretching direction and perpendicular to the MD (extrusion direction of the original films).

Creep behaviour

The creep curves for the Pre-1 film at 30°C under different stresses and at three orientations (0°, 45° and 90°) are presented in *Figure 4a*, *b* and *c*, in which the creep strain is plotted against log time. For these curves, the open symbols represent experimental data points, and the solid lines have been drawn using the best fit according to equation (1). At each orientation, a higher stress resulted in a larger initial creep strain and a larger creep rate (upward curvature at the end of the creep curves). At the same stress level, samples at different orientations with respect to the MD also showed different initial creep strains and plateau creep rates, with the 90° orientation being the least, followed by the 0° and finally the 45° orientation displaying the highest creep rate. Data presented in these figures have been well reproduced by using another set of samples at each of the orientation angles.

DTMA data, which is related to the creep rate, for Pre-1 film at 30°C are shown in *Figure 4d*, *e* and *f*, where creep

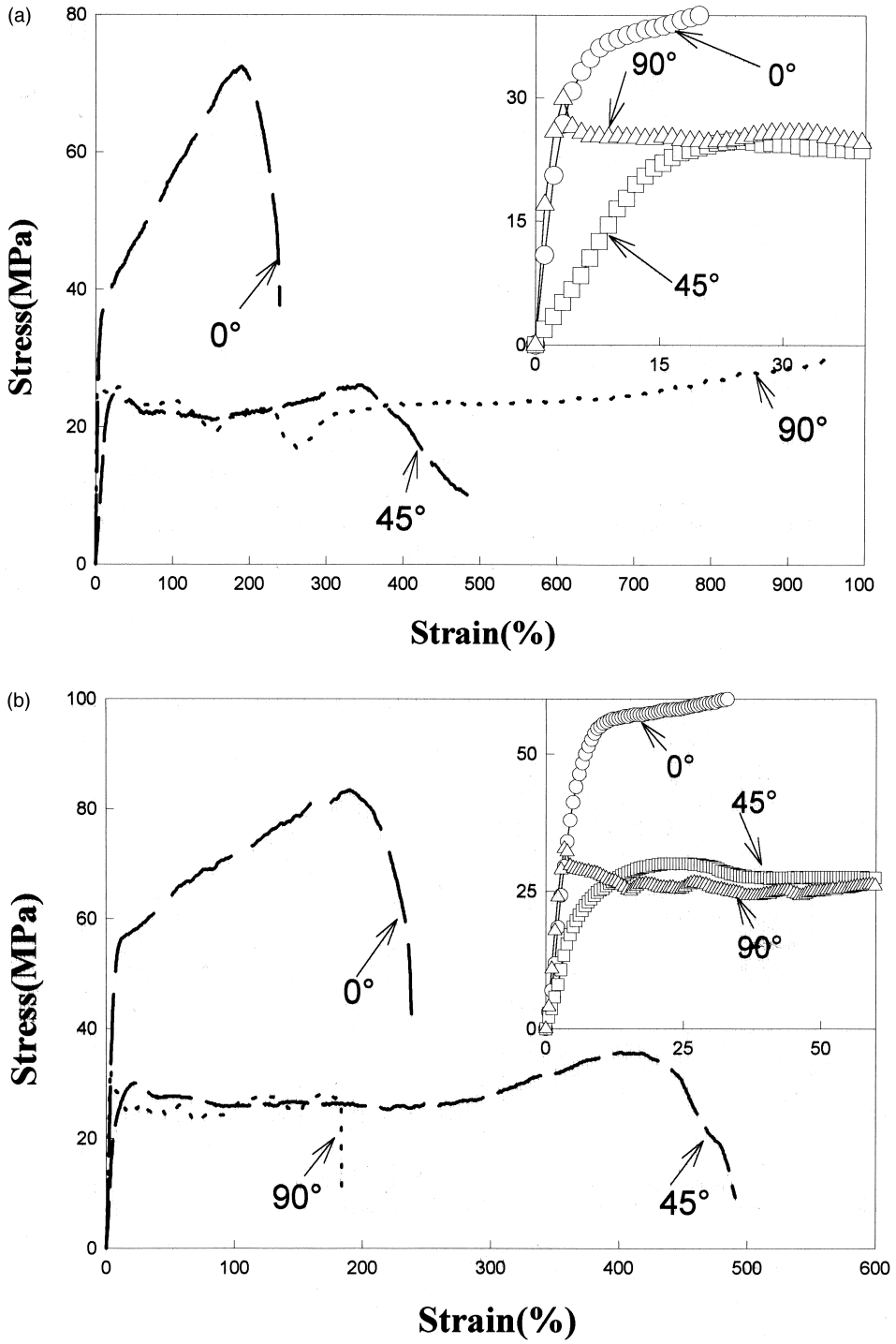

Figure 3 Stress–strain curves for the Pre-1 (a) and Pre-2 (b) films at the designated three orientations

rate (calculated from the DTMA data) is plotted against the creep strain. The open symbols and solid lines in these curves have the same meaning as mentioned previously. It can be clearly seen that at long loading times, a plateau creep rate is indeed achieved for each individual creep experiment. Additionally, it can be seen that the curve fitting according to equation (1) is quite good in terms of providing values for the *creep rate at longer times*, although this model is not a good approximation at the earlier stages of the experiment. We noticed that the scattering of the DTMA data in *Figure 4f* at larger strains is bigger, but the curve fit is at the mean value of these data. The creep rate used hereafter was obtained from the best fit according to equation (1).

The creep curves for the Pre-1 film at 60° under different stresses and at the 0° and 90° orientations are shown in *Figure 5a* and *b*. The creep strain for the 45° orientation at this high temperature, as well as at 40°C and 50°C, was too large to be accurately measured by the TMA instrument used in this study, and is therefore not available. Again, a higher stress resulted in a larger creep strain and creep rate as expected. At the same stress level, the creep strain for the 90° orientation is less than that for the 0° orientation, and so is the creep rate. Furthermore, in the case of 90° creep, a neck developed during the creep experiment at the highest stress level used; when this occurs, the creep curve dramatically undergoes a rapid rise. The creep rates, either

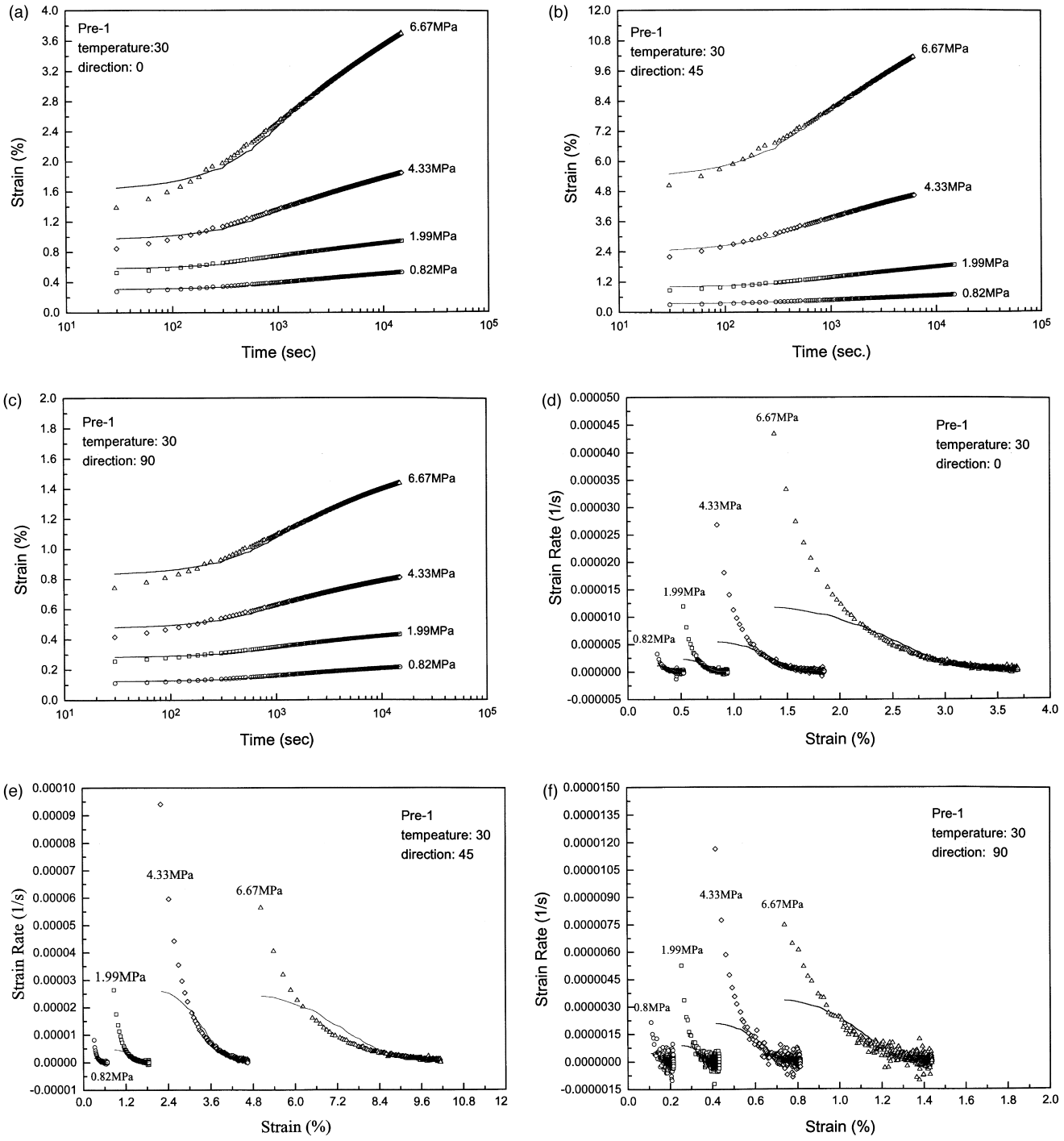

Figure 4 Creep (TMA) data (a–c) and DTMA data (d–f) for the Pre-1 film at 30°C and three directions of 0°, 45° and 90°

from the fitting according to equation (1) or calculated from the DTMA data, are presented in *Figure 5c* and *d* for the respective 0° and 90° creep. Again, the validity of curve fitting at longer loading times is confirmed. For the 90° creep at the highest load (60 g and 6.67 MPa for stress), fitting was not performed due to the presence of the significant rise of creep rate at the end of the experiment, as shown in *Figure 5b* and *d*.

The creep response of the Pre-2 film at 30°C and 60°C are presented in *Figures 6 and 7* where creep strain is plotted against time. The data essentially display the same trend as explained above for the case of the Pre-1 film. *Figures 8 and 9* present the same linear plots at both 30°C and 60°C for the HP-1 and HP-2 films, respectively; here molecular orientation is not a concern. Since the creep experiment is limited by the TMA instrument (100 g is the maximum load), the highest stresses for the compression moulded films were less than that for the thinner melt-extruded films. Nevertheless, the initial creep strains under similar stress level are comparable between melt-extruded films and compression moulded films, and this provides a base for the comparison between the creep data for melt-extruded films and compression moulded films (see later discussion).

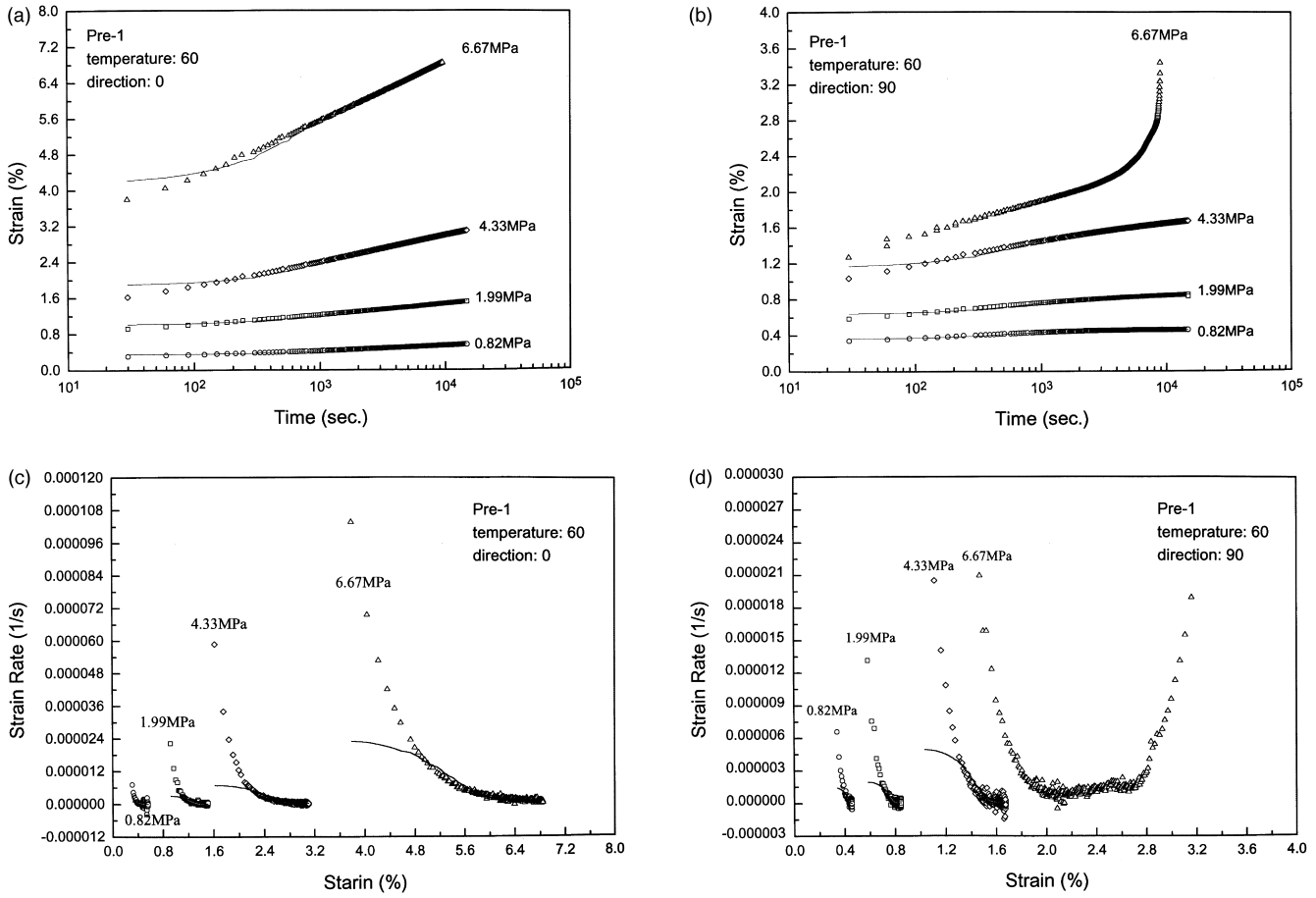

Figure 5 Creep (TMA) data (a and b) and DTMA data (c and d) for the Pre-1 film at 60°C and two directions of 0° and 90°

Table 1 Creep parameters, activation volume, activation energy and population of creep sites, obtained by applying an Eyring-rate analysis (equation (2)) for the Pre-1, Pre-2, HP-1, and HP-2 films

Parameters	Pre-1			Pre-2			HP-1	HP-2
	0°	45°	90°	0°	45°	90°		
V (nm^3)	1.93 ± 0.28	2.20 ± 0.34	1.92 ± 0.31	1.52 ± 0.26	1.71 ± 0.30	1.56 ± 0.28	1.73 ± 0.4	1.60 ± 0.38
U (kJ mol^{-1})	22.1 ± 2.5	[a]	23.8 ± 2.8	25.1 ± 2.9	[a]	28.3 ± 2.2	5.5 ± 1.1	4.9 ± 0.8
$\dot{\epsilon}_o$ (s^{-1})	1.59	[a]	0.4	2.0	[a]	0.3	0.007	0.006

[a]Not available due to the lack of creep data at temperatures higher than 30°C at the 45° direction

Creep parameters obtained form the Eyring-rate equation

The three parameters, namely activation volume (V), activation energy (U), and the availability of creep sites ($\dot{\epsilon}_o$), in the Eyring-rate equation were obtained by fitting the creep rates to equation (2). The creep rate at different temperatures, stresses, and loading orientations with respect to the MD were obtained by the best fit based on equation (1), as already shown previously. A similar form of curve fitting has been done in the creep studies for highly oriented HDPE fibres studied by Ward and coworkers[21–23] and UHMWPE fibres by Pennings[24]. In their cases, since the applied stress was on the order of 1 GPa and the value of (V/kT is usually larger than 3[21–25,31], the hyperbolic sine function was simplified as a exponential function, i.e. $\sinh(X) \approx 0.5\exp(X)$ at $X \geq 3.0$. In our study, however, the applied stress in the creep experiments is on the order of 1 MPa; therefore, the exact expression of the hyperbolic sine function has to be utilized.

The fitting procedures can be illustrated by using the Pre-1 film as an example: activation volume (V) was obtained by fitting the creep rate at the same temperature but different stress (*Figure 10a–c*) to equation (2), and the values shown in these figures are the average values at different temperatures. On the other hand, the activation energy (U) was obtained by plotting the creep rate (in logarithmic scale) *versus* reciprocal temperature (*Figure 10d* and *e*) at different stress levels, and the values shown in these plots are the average values at different stresses. Finally, the fitting necessary for obtaining $\dot{\epsilon}_o$ was performed by plotting the creep rate (in logarithmic scale) against $\log(\exp(-U/kT)\sinh((V/kT))$ (*Figure 10f* and *g*). Notice that the data are not perfectly linear but rather are more sigmoidal in shape which is very similar to the data presented by Ward *et al.*[32]. The results for the best fit for V, U and $\dot{\epsilon}_o$ for the melt-extruded compression moulded films are listed in *Table 1*. As stated earlier, the parameters of U

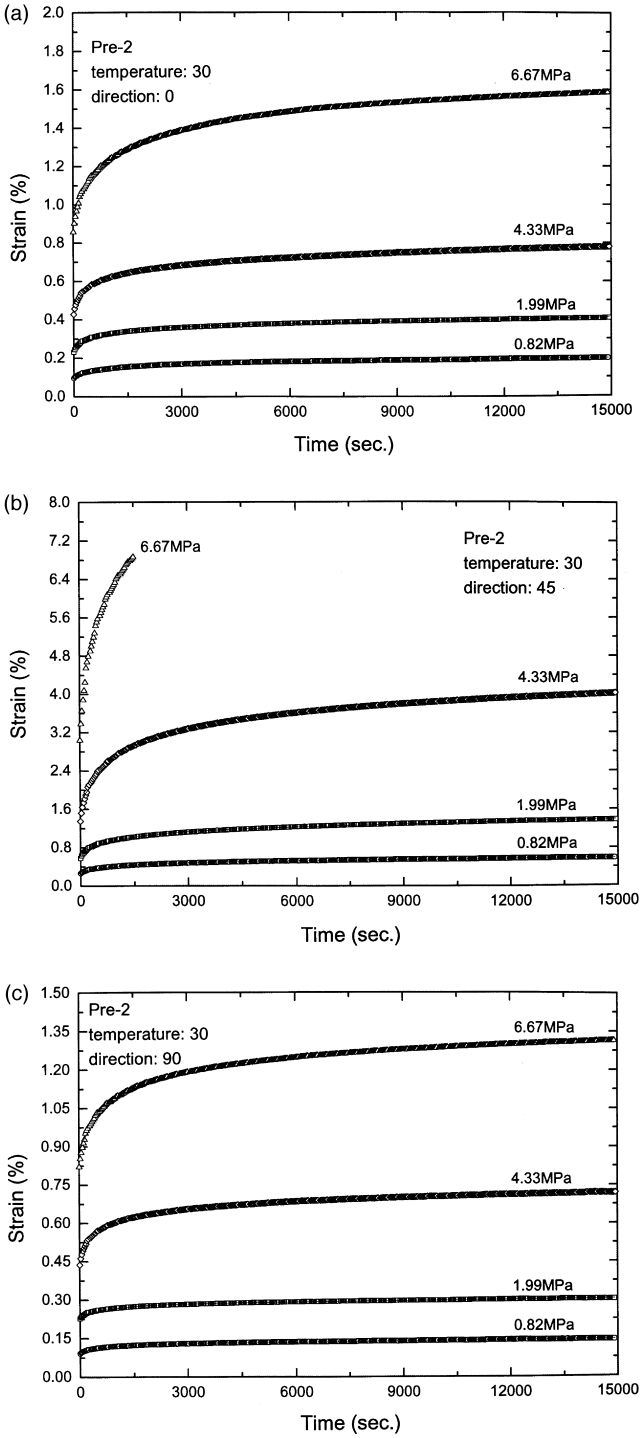

Figure 6 Creep (TMA) data (a–c) for the Pre-2 film at 30°C and three directions of 0°, 45° and 90°

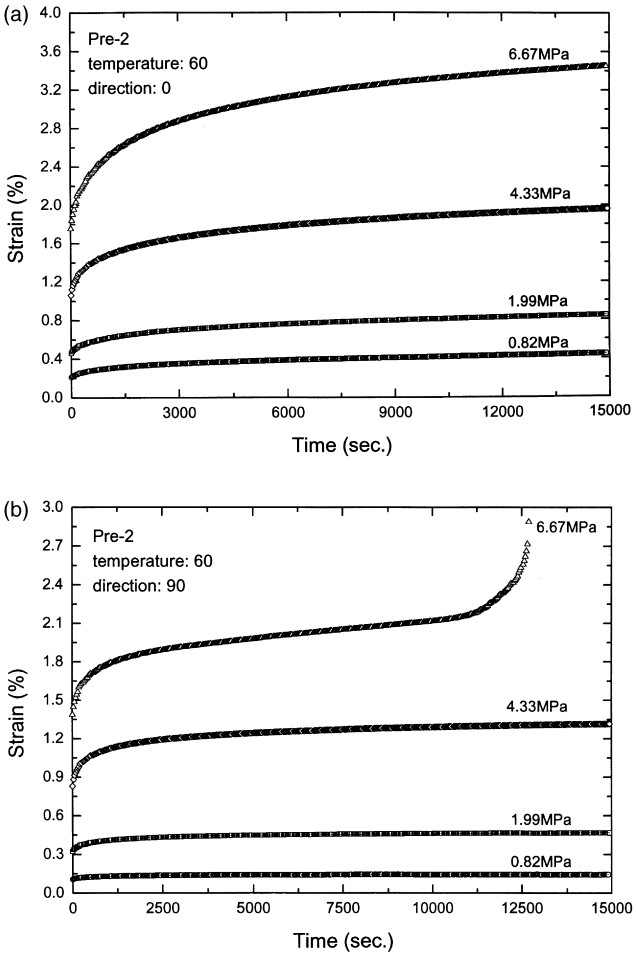

Figure 7 Creep (TMA) data (a and b) for the Pre-2 film at 60°C and two directions of 0° and 90°

and $\dot{\epsilon}_o$ for the creep in the 45° direction of the Pre-1 and Pre-2 films were not available due to the lack of creep data at temperatures higher than 30°C at this particular loading direction.

DISCUSSION

Creep behaviour of the melt-extruded HDPE films

It has been mentioned earlier that the samples at different orientation with respect to the MD displayed different creep behaviour. Shown in each of *Figure 11a* and *b* are three creep curves for the Pre-1 and Pre-2 films under the same stress of 0.82 MPa and at the same temperature of 30°C for the 0°, 45° and 90° orientations. The major differences between these curves are the initial strain and the plateau creep rate, which will be addressed separately.

Generally, the initial strain of a given creep curve reflects the instantaneous elastic response of the sample and therefore is dependent on its Young's modulus. For the Pre-1 and Pre-2 films, the crystalline lamellae are highly oriented with their normals preferentially aligned along the MD. Therefore, as a first approximation, the materials can be crudely considered as laminated composites of a hard crystalline phase and a soft amorphous phase stacked along the MD. The modulus of these melt-extruded films ('laminated composites') is certainly dependent on the orientation of the deformation. At the 0° deformation, the material can be considered as the composite being deformed in an iso-stress case, i.e. the crystalline phase and the amorphous phase are deformed in series; therefore the modulus is dominated by that of the softer amorphous phase. On the other hand, at the 90° deformation, the material can be considered as the composite being deformed in an iso-strain case, i.e. the crystalline phase and the amorphous phase are deformed in parallel; therefore the modulus is dominated by that of the harder crystalline phase. Thus, although the modulus of the crystalline phase (lamellae) at the 90° orientation (perpendicular to the chain direction) is much less than that at the 0° orientation (parallel to the chain direction), the modulus for a *sample* at the 90° orientation is higher than that for a sample at the 0°

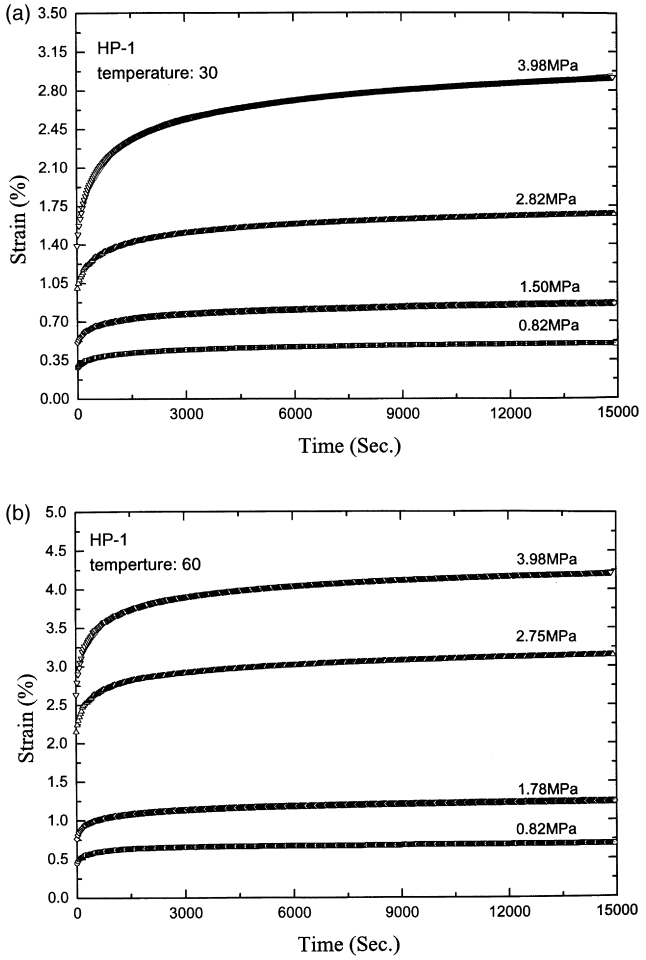

Figure 8 Creep (TMA) data for the HP-1 film at 30°C (a) and 60°C (b)

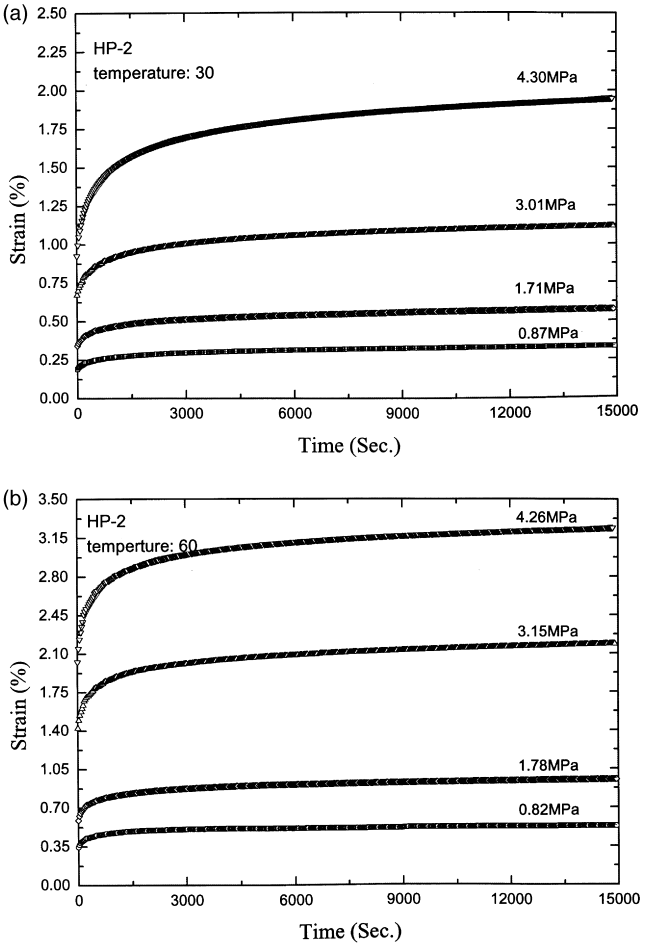

Figure 9 Creep (TMA) data for the HP-2 film at 30°C (a) and 60°C (b)

orientation. As for the 45° deformation, since there is a maximum resolved shear stress in the plane of the crystalline lamellae, interlamellar shear is the most probable deformation event, and this results in a even smaller modulus at this particular orientation. The different moduli at the three orientations can be seen directly by looking at the 'inserted' curves shown earlier in *Figure 3a* and *b* for the Pre-1 and Pre-2 films, respectively. It needs to be pointed out that the use of the 'laminated composite' model is only qualitative, since no consideration is given to chain tilt within the lamellae and the partial inclination of the lamellae stacks with respect to the MD.

The plateau creep rate can be understood based on the Eyring-rate model used in this study. According to equation (2), the creep rate is a function of three parameters—activation volume (V), activation energy (U) and the availability of creep sites ($\dot{\epsilon}_o$). From *Table 1*, for both the Pre-1 and Pre-2 films, the activation volume and activation energy for the 0° and 90° creep were about the same, and this implies that the molecular mechanisms involved at the two orientations are the same for both films. However, the availability of the creep sites is different at the two orientations—with the 0° creep being four and seven times larger than that for the 90° creep for the Pre-1 and Pre-2 films, respectively. This gives rise to a higher creep rate for the 0° creep than that of the 90° creep for samples under the same temperature and stress. As for the case of the 45° creep, the only parameter available was the activation volume at temperature of 30°C, and the value was also close to that for the 0° and 90° creep.

Creep mechanisms for the melt-extruded films

The activation energies for the Pre-1 and Pre-2 films listed in *Table 1* are much less than those reported for the UHMWPE fibres obtained by Ward *et al*. and Pennings *et al*. using the same approach[21–24]. However, small values of activation energy have also been reported by other authors, based on different approaches, for talc-filled polypropylene[19] and for HDPE[30] as obtained from creep studies carried out at small strains ($< 4\%$). Comparing the curves in *Figure 11a* and *b* (showing the orientation dependence of creep curves) with those in *Figure 3a* and *b* (showing the orientation dependence of stress–strain curves) that were obtained at similar temperatures, it can be seen that the final creep strains in *Figure 11* are clearly less than the corresponding yield strains in *Figure 3* for both the Pre-1 and Pre-2 films, except for the 90° creep at 60°C where the final creep strain rises to the corresponding yield point and, because of this, sample failure occurred. For HDPE materials, the amorphous phase has a T_g much lower than the temperatures used in the creep study; therefore, the amorphous phase, or at least a very major portion of it, is in a rubbery state. Under external tensile loading, it is likely that the initial response of the material is the deformation of the amorphous phase, and crystalline phase will not contribute greatly to creep under these conditions until the deformation of the amorphous is highly constrained, such as near the yield point[33]. The existence of the fibril structures for the Pre-2 films can limit the amount of pre-yielding deformation; however, the deformation of the amorphous phase is not expected to be totally prohibited. This is the

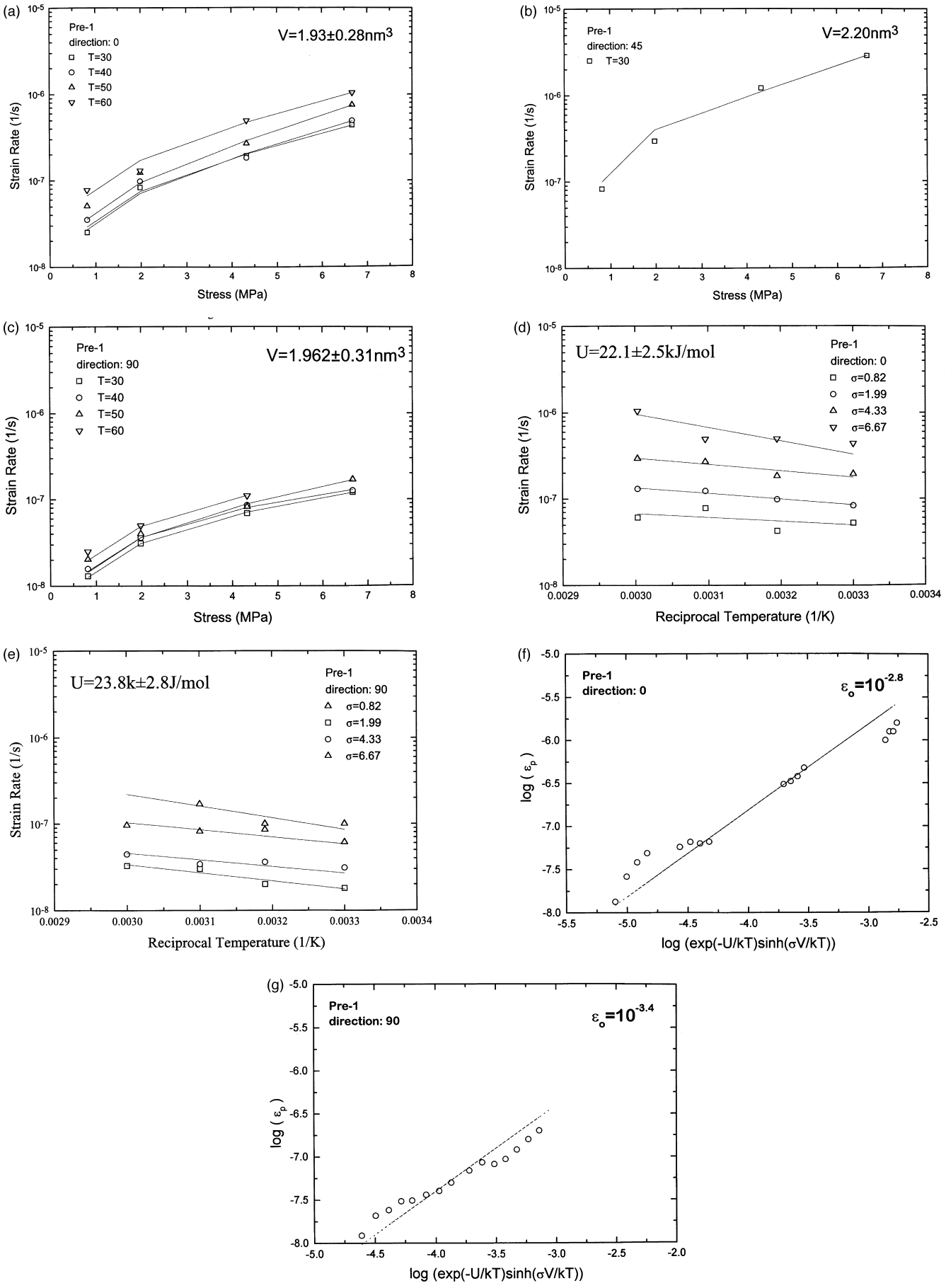

Figure 10 Activation volume (a–c), activation energy (d and e) and pre-exponential factor (f and g) based on the fitting according to equation (2) for the Pre-1 film

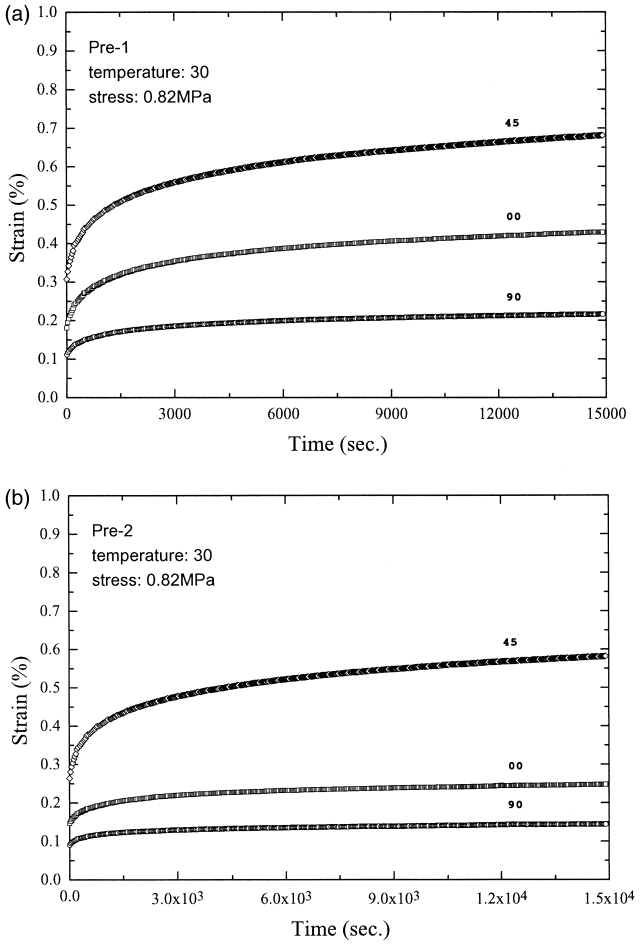

Figure 11 Creep curves for the Pre-1 (a) and Pre-2 (b) films at three directions of 0°, 45° and 90° at 30°C and 0.82 MPa

reason that the calculated activation energy in this study (5–30 kJ mol^{-1}) is much less than the typical values for the deformation of the crystalline phase, in the region of 100–200 kJ mol^{-1} for polyethylene[34].

Generally, at least three different kinds of amorphous regions need to be addressed[35], these being: (1) relaxed chains that are in the random coil state; (2) cilia that are suspended from the chain-folding surface of the crystalline lamellae; and (3) tie-chains that connect adjacent crystalline lamellae. Among them, the tie-chains deserve the most attention, because they may act as load transfer agents between the crystalline lamellae, although some relaxed chains can also contribute to the load transfer due to trapped entanglements. There have been several investigations on tie-chains in semicrystalline polymers by using small angle neutron scattering (SANS), nuclear magnetic resonance (n.m.r.), and mechanical testing[36–46]; however, a complete understanding regarding the full role of tie-chains is premature and limited at present.

We believe that three fundamental parameters that are important for the influence of tie-chains on creep behaviour are enthalpy, entropy, and number density. The first two parameters can be and have been referred to as the 'tautness' of the tie-chains, i.e. the more taut the tie-chains are, the higher enthalpy and the less entropy they have. The number density of the tie-chains can be influenced by many factors, such as molecular weight and its distribution, amount of short branches and their distribution in a given backbone, crystallization conditions, etc. Tie-chain density has been estimated by different methods according to different authors[36–46]; however, the energy state (combination of enthalpy and entropy) of the tie-chains has not yet been addressed in the literature.

As mentioned earlier, the creep strain in the melt-extruded films is in the pre-yielding region in which amorphous deformation is dominant; therefore, it is reasonable to believe that the tie-chains are the principal structural unit that determine the pre-yield creep behaviour of these films. Since the same tie-chain networks controls the creep deformation for both the 0° and 90° creep, the activation volume and activation energy should be identical, as shown by the data in *Table 1*. However, the availability of the creep sites are different. This can be explained by the constraint effect of the crystalline lamellae on the tie-chains. For the 0° creep, all the possible creep sites (non-taut tie-chains) may become partially activated due to the separation of crystalline lamellae under loading. However, for the 90° creep, since the crystalline lamellar separation is not the major deformation event, a major fraction of tie-chains would not transfer load; therefore, this portion of tie-chains are unlikely to be active—resulting in a lower number of available creep sites for the 90° creep than that for the 0° creep. In the case of the 45° creep, even the taut tie-chains can be activated due to the interlamellar shear motion and therefore the available creep sites is the largest, and this is conjectured to be the reason that at this particular orientation the creep rate is the highest, although the activation energy is not known.

The creep parameters for the Pre-1 and Pre-2 films listed in *Table 1* tend to imply that a trend exists for the occurrence of a smaller activation volume for the Pre-2 than that for the Pre-1 film and for a larger activation energy for the Pre-2 film than that for the Pre-1 film, although the differences are not significant in a statistical analysis. If, however, we accept these trends, we conjecture that these may be possibly explained by the different physical state of the tie-chains in the two films. Since the Pre-2 film has a wider molecular weight distribution (with the same number average molecular weight) than the Pre-1, it is expected that the tie-chain density for the Pre-2 film is higher than that for the Pre-1 film[47] and therefore gives rise to a smaller activation volume. In the process of melt extrusion, the broader molecular weight distribution for the Pre-2 film imparts a significantly longer relaxation time, as compared with that of the Pre-1 film as has been quantified in ref. 28. This longer relaxation time promotes the distinct presence or higher concentration of well defined row nucleated structures in the Pre-2 film—in contrast, there is no visible sign (by TEM) of such structure in the Pre-1 film. Thus, it is possible that the tie-chains are in a higher orientation state (more taut state) in the Pre-2 films than are those in the Pre-1 film—corresponding to an higher activation energy. Although a previous study showed that the amorphous phase for both the Pre-1 and Pre-2 films is basically in an unoriented state[28], it does not necessarily exclude the existence of a small fraction of oriented (taut) tie-chains in the amorphous phase. Another possible reason for the higher activation energy for the Pre-2 film may be due to the contribution of the row-nucleated fibril structures. While the overall volume fraction of these structures is small, they can serve as 'pinning' structures to restrict lamellar separation under load. Hence, at small creep strain, these fibril structures will be activated and contribute to the creep process.

However, in general the creep behaviour for the Pre-1 and Pre-2 films are similar, quite unlike what has been found for

the case of large strain plastic deformation study carried out by the same authors for these same HDPE films[30]. Under larger strain deformation, these two films show very different yielding characteristics, cold-drawing behaviour and fracture response[30]. This leads the authors to conjecture that it might be possible that there are some trace amounts of row-nucleated fibril structures, which is much smaller in length (e.g. bridges), as part of the stacked lamellar morphology (in Pre-1 film). Such a structure can not be detected by TEM and WAXS due to its small amount. These bridges, if present, are expected to be more effective to influence the creep behaviour than they are for plastic deformation. One can speculate that these short bridges can restrict the opening of the amorphous regions between the crystalline lamellae under small creep strain, while the small aspect ratios of these bridges limit their strengthening effect under larger strain plastic deformation. In fact, in the general scheme of strain induced crystallization of polymer solutions or melts under shear stress proposed by Keller *et al.*[48], if their assumption is correct, it would seem necessary to have some type of linear or fibril nuclei to trigger the formation of the row-nucleated fibrils or stacked lamellar structure. Indeed, both the existence and precise nature of the row-nucleated fibril structures are still not fully understood[49–51].

General considerations of the creep behaviour for the unoriented HDPE materials

For the isotropic HP-1 and HP-2 films, which were intended to be used as examples for linear polyethylene crystallized under quiescent conditions, the calculated creep parameters listed in *Table 1* have some interesting features. First, the activation energy is only about 5kJ mol^{-1} (kT at room temperature is 2.6 kJ mol^{-1}). This extremely low activation energy imply that the tie-chains in the compression moulded materials are in a much less taut state, at least some portion of them, than those in the melt-extruded films, which can be justified by the different processing histories of these films. Another factor that can also help to explain this difference in activation energy is that 'shishes' or short bridges that are promoted in the strain induced morphologies from melt extrusion are not expected to be present in the compression moulded samples of the same resins. Second, the activation volumes are almost identical to those of melt extruded films, and this suggests that the processing (compression moulding *versus* melt-extrusion) does not greatly change the tie-chain density very much for these resins. This also implies that molecular weight and its distribution plays a critical role in terms of promoting tie-chains, as would be expected. Thirdly, the availability of creep sites for the compression moulded films is very sensitive to processing (crystallization) conditions—compression moulded films show much lower values than the melt-extruded films; this implies that the isotropic superstructure possessed by the compression moulded films provides much more of a constraint effect than the oriented stacked lamellar morphology in the melt-extruded films, possibly due to the radiating growth of the spherulitic structure. Certainly, such constraint effects must strongly depend upon such factors as the size of the superstructures, thickness of crystalline lamellae, crystallinity level, etc., which can be changed due to processing (crystallization) conditions.

For semicrystalline polymers at temperatures well above the T_g, if the creep strain is limited to below the yield point of the material, the creep behaviour is principally controlled by the deformation of the amorphous phase. For the case of HDPE materials, we have shown that regardless of the different morphologies (oriented stacked lamellar morphology either with or without distinct visibly observed row-nucleated fibril structure and an isotropic morphology), the creep behaviour can be reasonably described by the Eyring-rate model. As a result, this model also provides us some implications or further confirmation for approaches that may be or have been used to improve creep resistance, as will now be briefly addressed.

Two principal approaches that have been utilized in an attempt to improve the creep performance of high strength polyethylene are by either crosslinking the amorphous phase[32,52] or introducing branches into the linear chain[9,53]. Crosslinking in the solid state would increase tie-chain density, but it tends to sacrifice the tensile properties due to lower drawability of the crosslinked structure[54–59]. By introducing a small amount of short chain (e.g. butyl) branches along a linear polyethylene backbone by copolymerization of ethylene with another α-olefin (e.g. 1-hexene), besides lowering crystallinity, these short butyl branches also promote more tie-chains and, as a result, can improve creep behaviour[9].

Along the same lines, with a small amount of methyl branches which have been known to pack into the crystalline phase during the crystallization process[58–61], it has been found that the creep behaviour of ultra-high strength polyethylene fibres at a higher stress level is also improved[9]. It is argued that, for a polymeric crystal, creep strain is induced by a translational motion of polymer chains along the crystal *c*-axis within the crystalline phase, which is the same mechanisms as those that are responsible for the high temperature mechanical α relaxation in HDPE[9,10,62]. One can imagine that small amounts of methyl branches associated with the backbone chain *within the crystalline phase* can greatly limit the translational motion of the chain through the crystal lattice, and this lower chain mobility impairs a better creep resistance. The well-noted much higher creep resistance of poly-1-butene (compared with HDPE) has also been attributed to a much higher restriction of polymer chain motion within the crystal due to its bulkier butyl side groups along the backbone[63].

In this context, it needs to be pointed out that, in the creep studies of the high strength HDPE fibres, the creep at high stress is believed to be controlled by the deformation of the crystalline phase. Although the creep behaviour at low stress levels (3 GPa for fibres with Young's modulus of 100 GPa) is proposed to be due to the contribution from the amorphous entangled network, because of the high draw ratio and higher molecular weight, the amorphous phase is also speculated to be more oriented as well; thus the tie-chains are highly taut and highly constrained. Therefore, although the percent crystallinity is similar, the observed creep rate for these fibres is less than that obtained in our study.

CONCLUSIONS

The Eyring-rate model is found to describe the creep behaviour of the HDPE films with three different kinds of morphologies: a stacked lamellar morphology either with or without row-nucleated fibril structure and that with an unoriented isotropic morphology. The calculated activation volume for the HDPE films is in the order of 1–2 nm^3, and the activation energy is in the order of 20–30 kJ mol^{-1}, except for the compression moulded films which possess

activation energies of *ca* 5 kJ mol^{-1}. For all the experiments, the creep behaviour of these films is believed to be controlled by the deformation of amorphous phase, more specifically the tie-chains. The dependence of the creep behaviour on loading direction for the melt-extruded films is more or less controlled by the difference in the availability of the creep sites at the different orientations. The creep at 90° has the lowest creep site availability, due to the highest constraint effects of the crystalline lamellae to the tie-chains followed by the creep at 0° and 45°, respectively. It was argued that the same constraint effect is a key to improve the creep resistance for isotropic materials (e.g. compression moulded films used in this study).

ACKNOWLEDGEMENTS

The authors would like to thank the Hoechst Celanese Co. for providing the melt-extruded HDPE films used in this study.

REFERENCES

1. Martin, J. and Pao, Y. H., *Proc. ASTM*, 1951, **51**, 1277.
2. Andrade, E. M., *Proc. Roy. Soc.*, 1970, **84**, 1.
3. Findley, W. N., *Polym. Eng. Sci.*, 1987, **27**, 582.
4. Vallat, M. F. and Plazek, D. J., *J. Polym. Sci., Phys. Ed.*, 1988, **26**, 555.
5. Ward, I. M., *Mechanical Properties of Polymers*, 2nd edn. John Wiley, NY, 1983.
6. Stephens, J. P., Ahmadieh, H. and Mukherjee, A., *J. Mater. Sci.*, 1978, **13**, 467.
7. Dixon-Stubbs, P. J., *J. Mater. Sci.*, 1981, **16**, 389.
8. Ohta, Y., Sugiyma, H. and Yasuda, H., *J. Polym. Sci., Phys. Ed.*, 1994, **32**, 261.
9. Komatsu, T. and Aoshima, A., *J. Polym. Sci., Phys. Ed.*, 1995, **33**, 179.
10. Findley, W. N., Lai, J. S. and Onaran, K., *Creep and Relaxation of Nonlinear Viscoelastic Materials*. Holland Publishing Co., Amsterdam, NY, 1976.
11. Buijs, J. A. H. M. and Vroge, G. J., *Polymer*, 1993, **34**, 4692.
12. Struik, L. C. E., *Physical Ageing of Amorphous Polymers and Other Materials*, Elsevier, Amsterdam, 1978.
13. Read, R. E., *J. Non-Cryst. Solids*, 1991, **131-133**, 408.
14. Lai, L. and Bakker, A., *Polymer*, 1995, **36**, 93.
15. Leblans, P. J. R. and Bastiaansen, W.M., *J. Polym. Sci., Phys. Ed.*, 1989, **27**, 1009.
16. Bhuvanesh, Y. C. and Gupta, V. B., *Polymer*, 1995, **36**, 3669.
17. Struik, L. C. E., *Polymer*, 1987, **28**, 1251.
18. Struik, L. C. E., *Polymer*, 1989, **30**, 799.
19. Trantina, G. G., *Polym. Eng. Sci.*, 1986, **26**, 776.
20. Erying, H., *J. Chem. Phys.*, 1936, **4**, 238.
21. Wilding, M. A. and Ward, I. M., *Polymer*, 1978, **19**, 969.
22. Wilding, M. A. and Ward, I. M., *J. Mater. Sci.*, 1984, **19**, 629.
23. Ward, I. M. and Wilding, M. A., *J. Polym. Sci., Phys. Ed.*, 1984, **22**, 561.
24. Penning, J. P., Pras, H. E. and Penning, A., *J. Coll. Polym. Sci.*, 1994, **272**, 664.
25. Sengonul, A. and Wilding, M. A., *Polymer*, 1995, **36**, 4579.
26. Allen, S. R. and Roche, E. J., *Polymer*, 1989, **30**, 996.
27. Rogozinsky, A. K. and Bazhenov, S. L., *Polymer*, 1992, **33**, 1391.
28. Yu, T. and Wilkes, G. L., *J. Rheo.*, 1996, **40**, 1079.
29. Yu, T. and Wilkes, G. L., *Polymer*, 1996, **37**, 4675.
30. Zhou, Hongyi and Wilkes, G. L., *J. Mater. Sci.*, 1998, **33**, 287.
31. Govaert, L. E. and Lemstra, P. J., *Coll. Polym. Sci.*, 1992, **270**, 455.
32. Wilding, M. A. and Ward, I. M., *Polymer*, 1981, **22**, 870.
33. Bartczak, Z., Galeski, A., Argon, A. S. and Cohen, R. E., *Polymer*, 1996, **37**, 2113.
34. Boyd, R. H., *Polymer*, 1985, **26**, 323.
35. Yoon, D. Y. and Flory, P., *Polymer*, 1977, **18**, 509.
36. Heith, H. D., Padden, F. J. Jr and Vadimsky, R., *J. Polym. Sci., Phys. Ed.*, 1980, **18**, 2307.
37. Brown, N. and Ward, I. M., *J. Mater. Sci.*, 1983, **18**, 1405.
38. Lustiger, A. and Markham, R. L., *Polymer*, 1983, **24**, 164.
39. Fischer, E. W., Hahn, K., Kugler, J., Struth, U. and Born, R., *J. Polym. Sci., Phys. Ed.*, 1984, **22**, 1491.
40. Zhizhenkov, V. V. and Egorv, E. V., *J. Polym. Sci., Phys. Ed.*, 1984, **22**, 117.
41. Bhattacharya, S. K. and Brown, N., *J. Mater. Sci.*, 1985, **20**, 2767.
42. Huang, Y. L. and Brown, N., *J. Polym. Sci.*, 1990, **28**, 2007.
43. Yeh, J. T. and Runt, J., *J. Polym. Sci., Phys. Ed.*, 1991, **29**, 371.
44. Huang, Y. L. and Brown, N., *J. Polym. Sci., Phys. Ed.*, 1991, **29**, 129.
45. Bohm, L. L., Enderle, H. M. and Fleirner, M., *Adv. Mater.*, 1992, **4**, 234.
46. O'Connell, P. A., Bonner, M. J., Duckett, R. A. A. and Ward, I. M., *Polymer*, 1995, **36**, 1995.
47. Huang, L. Y. and Brown, N., *J. Mater. Sci.*, 1988, **23**, 3648.
48. Keller, A. and Mackley, M. R., *Pure Appl. Chem.*, 1974, **39**, 195.
49. Salazar, J. M., Ramos, J. V. G. and Petermann, J., *Inter. J. Polymeric Mater.*, 1993, **21**, 111.
50. Pennings, A. J., Von der Mark, J. M. A. A. and Booij, H. P., *Koll. Z. Z. Polym.*, 1970, **236**, 99.
51. Grubb, D. T. and Mill, M. J., *J. Crystal Growth*, 1980, **48**, 321.
52. Hikmet, R., Lemstra, P. J. and Keller, A., *Coll. Polym. Sci.*, 1987, **265**, 185.
53. McFaddin, D. C., Russell, K. E. and Kelusky, E. C., *Polym. Commun.*, 1988, **29**, 258.
54. Ijkstra, D. J., Krischbaum, R. and Pennings, A. J., *Polymer*, 1989, **30**, 866.
55. Matsuo, M. and Sawatari, C., *Macromolecules*, 1986, **19**, 2028.
56. Hikmet, R., Lemstra, P. J. and Keller, A., *Colloid Polym. Sci.*, 1987, **265**, 185.
57. Boer, J. De., Van den Berg, H. J. and Pennings, A. J., *Polymer*, 1978, **19**, 969.
58. Swan, P. R., *J. Polym. Sci.*, 1962, **56**, 409.
59. Walter, F. R. and Reading, F. P., *J. Polym. Sci., Letter*, 1956, **99**, 561.
60. McFaddin, D. C., Russell, K. E. and Kelusky, E. C., *Polym. Commun.*, 1988, **29**, 258.
61. Hosoda, S., Nomura, H., Gotoh, Y. and Kihara, H., *Polymer*, 1990, **31**, 1999.
62. Zhou, Hongyi and Wilkes, G. L., *Macromolecules*, 1997, **30**, 4210.
63. Luciani, L., Sepala, J. and Lofgren, B., *Prog. Polym. Sci.*, 1988, **13**, 37.